Cerebral Cortex, August 2016;26: 3357–3369

doi:10.1093/cercor/bhv157
Advance Access Publication Date: 24 July 2015
Original Article

ORIGINAL ARTICLE

Regulation of Cortical Dynamic Range by Background Synaptic Noise and Feedforward Inhibition

Ayah Khubieh[1,2], Stéphanie Ratté[1,3], Milad Lankarany[1,3], and Steven A. Prescott[1,3]

[1]Neurosciences and Mental Health, The Hospital for Sick Children, Toronto, ON, Canada M5G 0A4, [2]School of Life Sciences, Ecole Polytechnique Fédérale de Lausanne (EPFL), Lausanne, Switzerland and [3]Department of Physiology and the Institute of Biomaterials and Biomedical Engineering, University of Toronto, Toronto, Canada

Address correspondence to Steven A. Prescott, Neurosciences and Mental Health, Hospital for Sick Children, 686 Bay Street, Toronto, ON, Canada M5G 0A4. Email: steve.prescott@sickkids.ca

Abstract

The cortex encodes a broad range of inputs. This breadth of operation requires sensitivity to weak inputs yet non-saturating responses to strong inputs. If individual pyramidal neurons were to have a narrow dynamic range, as previously claimed, then staggered all-or-none recruitment of those neurons would be necessary for the population to achieve a broad dynamic range. Contrary to this explanation, we show here through dynamic clamp experiments in vitro and computer simulations that pyramidal neurons have a broad dynamic range under the noisy conditions that exist in the intact brain due to background synaptic input. Feedforward inhibition capitalizes on those noise effects to control neuronal gain and thereby regulates the population dynamic range. Importantly, noise allows neurons to be recruited gradually and occludes the staggered recruitment previously attributed to heterogeneous excitation. Feedforward inhibition protects spike timing against the disruptive effects of noise, meaning noise can enable the gain control required for rate coding without compromising the precise spike timing required for temporal coding.

Key words: dynamic range, feedforward inhibition, gain control, noise, pyramidal neuron

Introduction

Neurons in the intact brain are constantly bombarded by synaptic input driven by ongoing network activity. That input causes increased membrane conductance, tonic depolarization, and noisy fluctuations in voltage (Holmes and Woody 1989; Bernander et al. 1991; Destexhe and Paré 1999; Destexhe et al. 2003). In comparison, neurons in brain slices experience little background input and are therefore less leaky, less depolarized, and less noisy. These effects have numerous consequences for neural coding. In pyramidal neurons, increased conductance affects spike initiation dynamics (Prescott et al. 2006; Prescott, Ratté, et al. 2008), which, in turn, affect phase locking properties (Broicher et al. 2012) and whether neurons receiving common input synchronize (Hong et al. 2012; Ratté et al. 2013). Other types of neurons are also affected (e.g., Wolfart et al. 2005). Increased membrane conductance, although initially thought to modulate firing rate gain (Eccles 1964; Blomfield 1974), was shown to shift the input–output (i–o) curve (Holt and Koch 1997). However, still later studies showed that membrane conductance does modulate firing rate gain but only under noisy conditions (Ho and Destexhe 2000; Chance et al. 2002; Longtin et al. 2002; Mitchell and Silver 2003; Prescott and De Koninck 2003; Shu et al. 2003; Cardin et al. 2008; Fernandez and White 2010). How background input affects gain—by causing increased conductance, noisy voltage fluctuations, and/or depolarization—has been debated but all 3 factors ultimately contribute and are not easily separated [Cardin et al. 2008; Prescott and De Koninck 2009; for review, see Silver (2010)]. Needless to say, background synaptic input has functionally important consequences.

It is, therefore, notable that response properties are often investigated in slice preparations that lack most of the background activity typical of the intact brain. Such experiments are valuable, but caution is warranted in their extrapolation to in vivo conditions. A case in point is the study by Pouille et al. (2009), which concluded that individual CA1 pyramidal neurons have a narrow dynamic range and that stimulus intensity is therefore encoded by the staggered recruitment of neurons rather than by the spike rate (or the probability of spiking) in any one neuron. According to their explanation, the population dynamic range is broad because of the broad distribution of neuronal i–o curve midpoints and despite the steepness of those curves. Staggered neuronal recruitment was shown to result from concomitant increases in synaptic excitation and inhibition combined with heterogeneities in synaptic excitation. Notwithstanding their rigorous demonstration, it remains uncertain whether the main finding of that study—the basis for a broad population dynamic range—applies to the intact, awake brain. Using dynamic clamp to recreate background synaptic input in brain slice experiments, together with mathematical modeling and computer simulations, we demonstrate here that individual pyramidal neurons have a broad dynamic range under realistically noisy conditions and that this noise effect, rather than the heterogeneity of synaptic excitation or cellular excitability, enables feedforward inhibition to regulate the population dynamic range. We show further that realistic noise levels do not preclude precise spike timing, thus leaving temporal coding intact. These results have important implications for understanding how the cortex achieves its prodigious capacity to encode information.

Materials and Methods

All procedures were approved by the Animal Care Committee at The Hospital for Sick Children. Adult male Sprague–Dawley rats (>28 days old) were deeply anesthetized with isoflurane and decapitated. The brain was rapidly removed to ice-cold oxygenated (95% O_2 and 5% CO_2) sucrose-substituted artificial CSF (ACSF) containing (in mM) 252 sucrose, 2.5 KCl, 2 $CaCl_2$, 2 $MgCl_2$, 10 glucose, 26 $NaHCO_3$, 1.25 NaH_2PO_4, and 5 kynurenic acid. Using a VT-1000S microtome (Leica), 400-μm-thick coronal slices were prepared and thereafter kept in normal oxygenated ACSF (126 mM NaCl instead of sucrose and without kynurenic acid) at room temperature until recording. Slices were transferred to a recording chamber perfused with oxygenated (95% O_2 and 5% CO_2) ACSF heated to 31 ± 1 °C and viewed with a Zeiss AxioExaminer microscope. Pyramidal neurons in CA1 hippocampus were recorded in the whole-cell configuration with >70% series resistance compensation using an Axopatch 200B amplifier (Molecular Devices). The pipette solution contained (in mM) 125 $KMeSO_4$, 5 KCl, 10 HEPES, 2 $MgCl_2$, 4 ATP (Sigma), 0.4 GTP (Sigma), as well as 0.1% Lucifer yellow; pH was adjusted to 7.2 with KOH. Pyramidal morphology was confirmed using epifluorescence after recording. Reported values of membrane potential are corrected for liquid junction potential. Responses were low-pass filtered at 2 kHz and digitized at 20 kHz using a Power1401 computer interface and Signal 5 software (Cambridge Electronic Design).

Signal

The input "signal" was applied in 1 of 2 ways: (1) Via synaptic input evoked by electrical stimulation of the Schaffer collaterals or (2) by virtual synaptic input applied directly to the recorded neuron via the patch pipette. In (1), a concentric bipolar electrode (FHC Inc.) was positioned on the Schaffer collaterals >500 μm from the recorded neuron and 100-μs-long stimuli were delivered at 0.05 Hz using a DS3 isolated constant current stimulator (Digitimer). Stimulus intensity was varied to span the entire dynamic range of each neuron. Ten stimuli were applied at each stimulus intensity for each testing condition (with vs. without added noise). In (2), synaptic transmission was blocked via bath application of (in μM) 10 CNQX, 40 D-AP-5, and 6 gabazine (Abcam), and virtual synaptic input was applied via dynamic clamp. Excitatory and inhibitory postsynaptic conductance (EPSG and IPSG) waveforms and their relative timing were based on Pouille et al. (2009). EPSG and IPSG vectors were normalized to a peak of 1 and then scaled by $\bar{g}_{\mathrm{excS}}$ or $\bar{g}_{\mathrm{inhS}}$, such that $\bar{g}_{\mathrm{excS}}$ and $\bar{g}_{\mathrm{inhS}}$ represent the peak of the EPSG and IPSG, respectively. Using dynamic clamp implemented through Signal 5 (CED), these inputs were applied to the neuron as signal current I_{Signal} according to the following equation:

$$I_{\mathrm{Signal}}(t) = \bar{g}_{\mathrm{excS}} \cdot \mathrm{EPSG}(t)(V(t) - E_{\mathrm{exc}}) + \bar{g}_{\mathrm{inhS}} \cdot \mathrm{IPSG}(t)(V(t) - E_{\mathrm{inh}})$$

where reversal potentials were $E_{\mathrm{exc}} = 0$ mV and $E_{\mathrm{inh}} = -70$ mV (which corresponds to +9 mV and −61 mV before correction for junction potential), and $\bar{g}_{\mathrm{inhS}}$ was fixed at 1.26 nS. Sixty stimuli were applied at 1.5 s intervals for each combination of $\bar{g}_{\mathrm{excS}}$ value and testing condition; this interval is long enough to ensure no interaction between consecutively applied signals.

Noise

Ornstein–Uhlenbeck processes (Uhlenbeck and Ornstein 1930) were used to construct noisy conductance waveforms that accurately approximate the synaptic bombardment experienced by pyramidal neurons in vivo (Destexhe et al. 2001). Noisy fluctuations in excitatory and inhibitory conductance (g_{excN} and g_{inhN}) are described by the following equations:

$$\frac{dg_{\mathrm{excN}}}{dt} = -\frac{g_{\mathrm{excN}}(t) - g_{\mathrm{exc0}}}{\tau_{\mathrm{exc}}} + \sqrt{\frac{2\sigma_{\mathrm{exc}}^2}{\tau_{\mathrm{exc}}}}\chi_{\mathrm{exc}}(t),$$

$$\frac{dg_{\mathrm{inhN}}}{dt} = -\frac{g_{\mathrm{inhN}}(t) - g_{\mathrm{inh0}}}{\tau_{\mathrm{inh}}} + \sqrt{\frac{2\sigma_{\mathrm{inh}}^2}{\tau_{\mathrm{inh}}}}\chi_{\mathrm{inh}}(t),$$

where χ is a random number drawn from a Gaussian distribution with 0 average and unit variance, while $\tau_{\mathrm{exc}} = 3$ mS and $\tau_{\mathrm{inh}} = 10$ ms in order to give appropriate autocorrelation structure. Other parameters were as follows: $g_{\mathrm{exc0}} = 1$ nS, $g_{\mathrm{inh0}} = 4$ nS, $\sigma_{\mathrm{exc}} = 0.6$ nS, and $\sigma_{\mathrm{inh}} = 1.5$ nS. These parameter values were chosen to produce membrane potential fluctuations of ~2 mV and spontaneous spiking at 2–5 Hz (measured in the absence of signal-evoked spiking) while roughly maintaining the excitation : inhibition ratios described by Destexhe and Paré (1999). Negative conductance values were rectified, so that only positive conductances were applied to the cell using dynamic clamp as noisy current I_{Noise} according to the following equation:

$$I_{\mathrm{Noise}}(t) = g_{\mathrm{excN}}(t)(V(t) - E_{\mathrm{exc}}) + g_{\mathrm{inhN}}(t)(V(t) - E_{\mathrm{inh}})$$

In a subset of experiments, constant background conductance was applied by setting σ_{exc} and σ_{inh} to 0 nS but keeping g_{exc0} and g_{inh0} at the values indicated above. Figure 1A illustrates sample voltage responses under control conditions and with noisy background input.

Exclusion Criteria

Measuring full i–o curves for multiple test conditions in each cell required >1 h of recording per neuron. Several steps were taken to

ensure the stability of recording conditions and cell properties during that period. Experiments were discontinued and data excluded if series resistance increased to >15 MΩ or if there was a qualitative change in spiking pattern elicited by square-wave stimulation. Furthermore, trials for different testing conditions were interleaved so as to avoid any systematic change in cellular excitability between testing conditions. Each neuron was typically tested under control conditions and 1 of 2 background conditions; accordingly, each noise condition was compared with control conditions using paired *t*-tests.

Analysis

Output was measured as the probability of spiking, P(spike), in response to signals (see above) applied multiple times at each intensity. The *i*–*o* curve for each testing condition in each neuron was fitted with a sigmoid of the form $y(x) = 1/(1 + e^{-(x-a)/b})$, where a represents the midpoint (or recruitment threshold) and $1/b$ represents the slope of the curve.

Computer Simulations

Simulations were conducted using a modified version of the Morris–Lecar model (Morris and Lecar 1981; Prescott et al. 2006; Prescott, De Koninck, et al. 2008) described by the following equations:

$$C\frac{dV}{dt} = -g_{Na} \cdot m_\infty(V)(V - E_{Na}) - g_K \cdot w(V - E_K) - g_{leak}$$
$$(V - E_{leak}) + I_{signal} + I_{noise}$$

$$\frac{dw}{dt} = \phi\frac{w_\infty(V) - w}{\tau_w(V)}$$

$$m_\infty(V) = \frac{1}{2}\left(1 + \tanh\left(\frac{V - \beta_m}{\gamma_m}\right)\right)$$

$$w_\infty(V) = \frac{1}{2}\left(1 + \tanh\left(\frac{V - \beta_w}{\gamma_w}\right) + a\left(1 - \tanh\left(\frac{V - \beta_{wa}}{\gamma_{wa}}\right)\right)\right)$$

$$\tau_w(V) = \frac{1}{\cosh\left(\frac{V - \beta_w}{2\gamma_w}\right)}$$

where $C = 2\ \mu F/cm^2$, $g_{Na} = 20\ mS/cm^2$, $E_{Na} = 50\ mV$, $g_K = 20\ mS/cm^2$, $E_K = -90\ mV$, $g_{leak} = 2\ mS/cm^2$, $E_{leak} = -67\ mV$, $\phi = 0.15$, $\beta_m = -11\ mV$, $\gamma_m = 20\ mV$, $\beta_w = -5\ mV$, $\gamma_w = 10\ mV$, $a = 0.05$, $\beta_{wa} = -55\ mV$, and $\gamma_{wa} = 8\ mV$. Signal was applied to model neurons using the same conductance waveform described above for experiments. The relationship between signal strength ($\bar{g}_{excS}$ and $\bar{g}_{inhS}$) and input intensity was varied, as described in the Results section. Background input was constructed the same way as for experiments, where $g_{exc0} = 0.4\ mS/cm^2$ and $g_{inh0} = 3.0\ mS/cm^2$ in order to reduce input resistance by ~50% and depolarize membrane potential by approximately 8 mV. For noisy background conditions, σ_{exc} and σ_{inh} were adjusted to produce voltage fluctuations with a standard deviation of 2.5 mV; for constant background conditions, σ_{exc} and σ_{inh} were adjusted to reproduce the small, 0.5-mV voltage fluctuations seen experimentally without added noise (see Results). All equations were integrated in XPPAUT (Ermentrout 2002) using the Euler method with a time step of 0.05 ms.

Results

Modest Background Noise Significantly Expands Neuron Dynamic Range

To mimic the noisy conditions present in vivo, we generated virtual synaptic conductances with Ornstein–Uhlenbeck processes

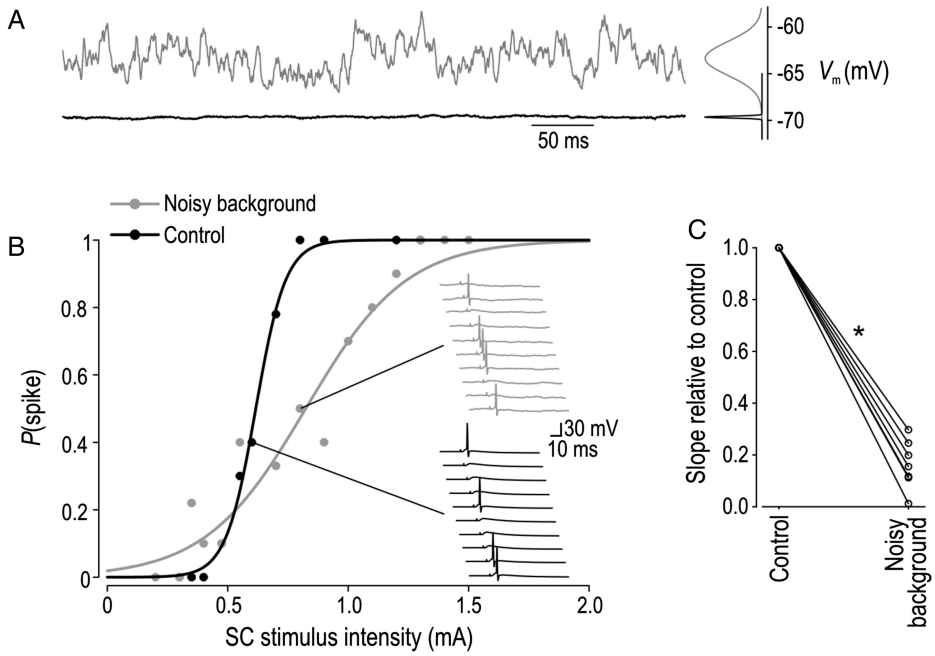

Figure 1. Effects of noise on responses to Schaffer collateral stimulation. (*A*) Sample traces under control conditions (black) and after introduction of fluctuating excitatory and inhibitory conductances that mimic background synaptic input (gray); no "signal" was applied. Difference in voltage distribution is summarized by fitted Gaussian curves shown on the right. (*B*) Input–output curves from a typical neuron tested with electrical stimulation of the Schaffer collaterals under control (black) and noisy background (gray) conditions. Insets show sample responses from which the probability of spiking was calculated. Data were fitted with a sigmoid from which the slope was measured. (*C*) Summary of the relative change in *i*–*o* curve slope attributable to noisy background. *$P < 0.05$, one-sample *t*-test.

(see Materials and Methods) and applied them to neurons via dynamic clamp. Figure 1A illustrates the impact of this noisy background input on membrane potential. We then measured the probability of spiking in response to real synaptic input triggered by Schaffer collateral stimulation. Figure 1B shows *i*–*o* curves and sample responses from a typical CA1 pyramidal neuron under control and noisy background conditions. Electrical stimulus intensity was not standardized across cells since we sought here only to compare between testing conditions within the same cell; instead, *i*–*o* curve slopes under noisy conditions are expressed relative to the *i*–*o* curve slope in the same neuron under control conditions (Fig. 1C). Relative slope was significantly reduced by introducing excitatory and inhibitory conductances that mimic noisy background synaptic input ($P < 0.05$; one-sample *t*-test).

In subsequent experiments, we replaced the input signal provided by Schaffer collateral stimulation with virtual EPSGs and IPSGs (Fig. 2A) constructed to mimic the direct excitation and feedforward inhibition elicited by Schaffer collateral stimulation (see Materials and Methods). This stimulation method has several benefits: (1) It ensures standardized signal strength since precisely controlled stimuli are applied directly to the recorded neuron, (2) it avoids causing synaptic plasticity, and (3) it allows the strength of excitatory and inhibitory signals ($\bar{g}_{\mathrm{excS}}$ and $\bar{g}_{\mathrm{inhS}}$) to be independently controlled. We held $\bar{g}_{\mathrm{inhS}}$ constant while varying $\bar{g}_{\mathrm{excS}}$ to isolate the effects of noise; as explained later (Figs 3–5), feedforward inhibition can interact with the effects of background noise or heterogeneous excitation to further expand the dynamic range.

Figure 2B shows the probability of spiking in a typical pyramidal neuron receiving dynamic clamp-based EPSGs and IPSGs under 3 conditions: control (i.e., without background), with noisy background, and with constant background. Relative to control conditions, slope was significantly reduced by the introduction of noisy background ($P < 0.001$, paired *t*-test), whereas slope was not significantly affected by introduction of constant background (Fig. 2C). Addition of constant background did, however, cause a significant leftward shift of the *i*–*o* curve midpoints ($P < 0.01$; paired *t*-test), as did noisy background ($P < 0.05$, paired *t*-test) although the latter effect was much smaller (Fig. 2D). Thus, whether activated by real or virtual synaptic input, the same neurons that exhibited a narrow dynamic range under the quiescent conditions present in vitro exhibited a much broader dynamic range under the noisy, high-conductance conditions that naturally exist in vivo and were reproduced here in vitro by dynamic clamp.

Figure 2E–G summarizes the effects of background input on passive membrane properties. Background input reduced input resistance by approximately 50%, caused depolarization of 6–8 mV, and produced voltage fluctuations with a standard deviation of approximately 2 mV in the case of noisy background. The magnitudes of these changes are conservative relative to in vivo data from CA1 neurons (Lee et al. 2006; Harvey et al. 2009; Epsztein et al. 2011) and neocortical pyramidal cells (see Introduction).

Mathematical Model Relating Population Dynamic Range to Neuron Recruitment and Neuronal Gain

The *i*–*o* curves for all recorded neurons are summarized in Figure 3A. As expected, *i*–*o* curves for control conditions were consistently steep, whereas those for noisy conditions were consistently shallower. The cumulative probability distribution of *i*–*o* curve midpoints was fitted with a sigmoid, the derivative of which describes the midpoint distribution (Fig. 3B). That distribution was much broader in control conditions than in noisy conditions. The broad midpoint distribution in control conditions is due entirely to heterogeneous cellular excitability (rather than to heterogeneous excitatory input) since all neurons received the same dynamic clamp signal. Notably, despite testing the same set of neurons in control and noisy conditions, the effects of heterogeneous excitability were absent under noisy conditions, which foreshadows a similar occlusion effect between noise and heterogeneous excitatory input (Fig. 5).

The population *i*–*o* curve is obtained by convolving the typical neuron *i*–*o* curve with the midpoint distribution. Or conversely, one can estimate the typical neuron *i*–*o* curve by deconvolving the population *i*–*o* curve with the midpoint distribution. Based on the midpoint distributions from experimental data in Figure 3B, we used the latter approach to predict the typical neuron *i*–*o* curve needed to yield a given population dynamic range (Fig. 3C) for comparison to measured *i*–*o* curves in Figure 3A. The neuron *i*–*o* curves thus derived correctly predicted the shape of measured *i*–*o* curves for the corresponding test condition. This demonstrates that an equivalent population dynamic range can be achieved in 2 ways: Through a broad distribution of steep neuron *i*–*o* curves or through a narrow distribution of shallow neuron *i*–*o* curves.

The breadth of the midpoint distribution and neuron dynamic range affects whether those factors are susceptible to modulation by feedforward inhibition whose strength co-varies with synaptic excitation (Fig. 3D). For sake of argument, imagine that individual neurons have infinitely steep *i*–*o* curves (and thus an infinitesimally narrow dynamic range) and, therefore, that the broad population dynamic range is achieved entirely on the basis of broadly distributed neuron *i*–*o* curves. In this scenario, the strength of inhibition cannot increase across the infinitesimally narrow dynamic range of any one neuron, and thus, it fails to expand the neuron dynamic range. On the other hand, the strength of inhibition will increase (in proportion to excitation) across the broad midpoint distribution, and thus, it will expand that distribution. This scenario—broad midpoint distribution combined with steep neuron *i*–*o* curves—most closely approximates control conditions and predicts that in the absence of noise, inhibition will expand the population dynamic range entirely by delaying the staggered recruitment of neurons (i.e., expanding the midpoint distribution). In contrast, under noisy conditions, where the midpoint distribution is narrow and neuron *i*–*o* curves are shallow, inhibition will expand the population dynamic range by expanding the dynamic range of individual neurons. The population dynamic range is sensitive to modulation of either of its underlying factors—the shape and distribution of neuron *i*–*o* curves—but, as illustrated by the simple mathematical model presented in Figure 3, those factors are themselves differentially sensitive to modulation by inhibition depending on background noise.

Relative Contribution of Staggered Neuron Recruitment and Neuronal Gain to the Population Dynamic Range

Next, we used computer simulations to disentangle the effects of heterogeneous excitation, noisy background input, and feedforward inhibition on the population dynamic range. First, we reproduced in our neuron model the changes in passive membrane properties caused by background synaptic input (see Materials and Methods). Using those background input parameters, we then compared between heterogeneous excitation under constant background conditions (Fig. 4, left column) and

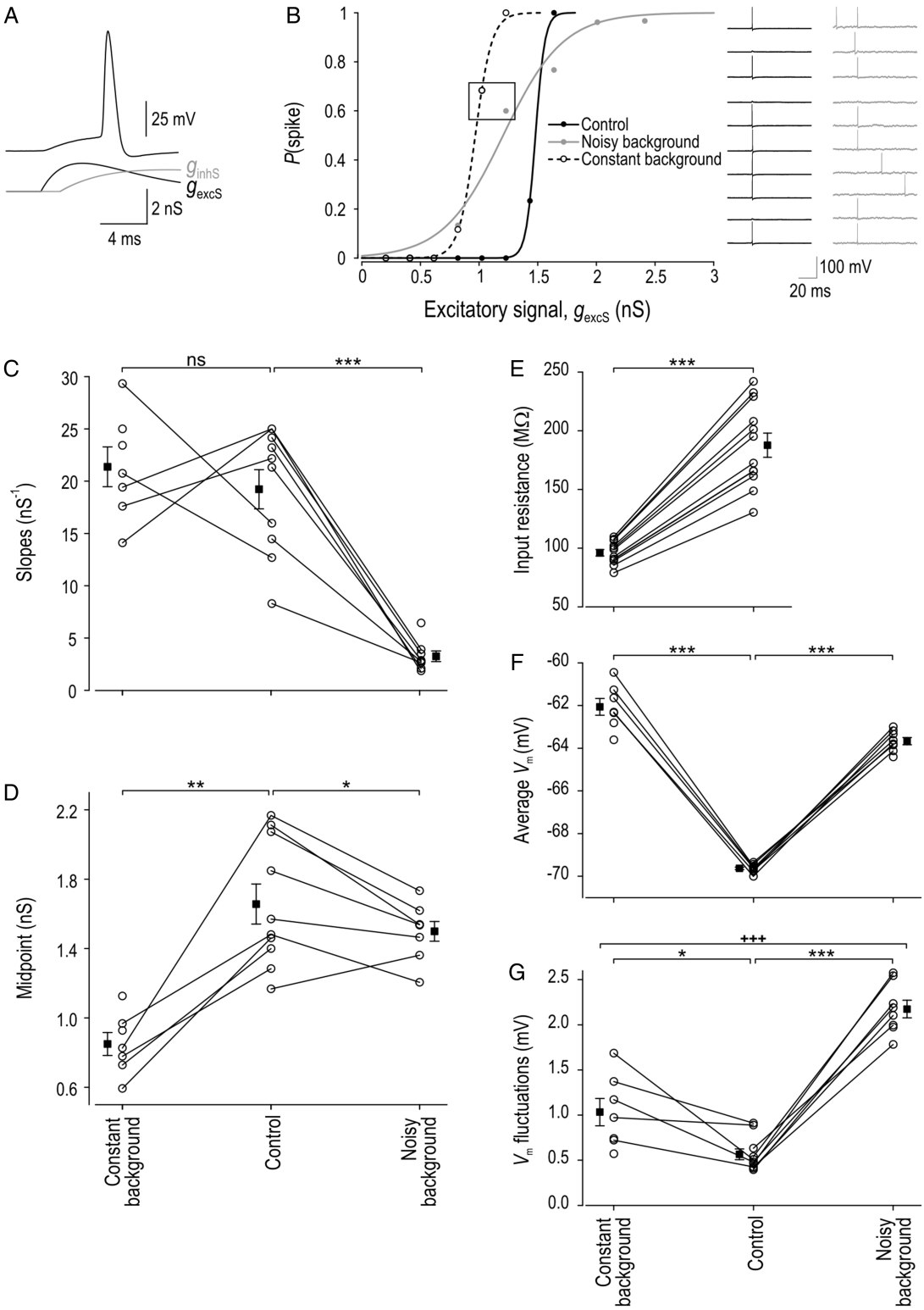

Figure 2. Effects of noise on responses to dynamic clamp-based input. (*A*) Example of a spike (top) evoked by the excitatory signal (g_{excS}, black) and inhibitory signal (g_{inhS}, gray) applied using dynamic clamp. The conductance waveforms and their relative timing are based on Pouille et al. (2009). (*B*) Input–output curves from a typical neuron tested under control conditions (solid black), after introduction of noisy background conductance (gray), and after introduction of constant background conductance (dashed black). Inset shows sample responses corresponding to boxed data points on left. (*C*) Summary of change in i–o curve slope from all neurons analyzed. For *C*–*G*, data points are shown for each neuron tested (open circles) together with the mean ± SEM for each condition (black squares). (*D*) Summary of change in i–o curve midpoint from all neurons analyzed. Summary of input resistance (*E*), average membrane potential (*F*), and membrane potential fluctuations (*G*). ***$P < 0.001$; **$P < 0.01$; *$P < 0.05$; ns, not significant; paired *t*-tests. $^{+++}P < 0.001$; unpaired *t*-test.

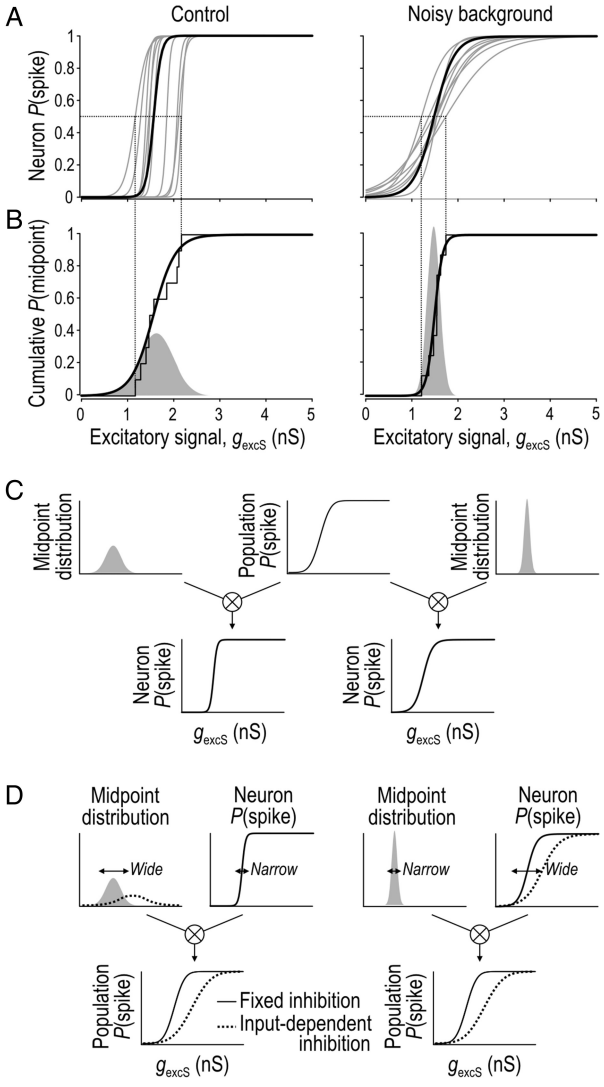

Figure 3. Mathematical model linking the population dynamic range to neuronal gain and midpoint distribution. (*A*) Gray curves show the *i*–*o* curve measured for each neuron tested with virtual EPSGs and IPSGs under control and noisy background conditions. Black curve shows the *i*–*o* curve calculated in *C*. Dotted lines highlight the distribution of midpoints. (*B*) Cumulative probability distribution of midpoints fitted with a sigmoid, the derivative of which gives an approximation of the midpoint distribution shown as a shaded curve. (*C*) We calculated the typical neuron *i*–*o* curve (bottom panels) needed to produce a given population *i*–*o* curve (top center panel) by deconvolving the population *i*–*o* curve with the midpoint distributions measured in *B* (top side panels). The neuron *i*–*o* curves thus obtained match the shape of measured neuron *i*–*o* curves in *A*. These data show that a broad population dynamic range can be achieved on the basis of steep but broadly distributed neuron *i*–*o* curves ("control conditions") or on the basis of narrowly distributed but shallow neuron *i*–*o* curves ("noisy background conditions"). (*D*) Explanation of how relationships in *C* impact modulation by inhibition. Even if $\bar{g}_{inhS}$ co-varies with $\bar{g}_{excS}$, $\bar{g}_{inhS}$ will not significantly increase across (and therefore cannot modulate) the neuron dynamic range if the dynamic range is narrow; consequently, under control conditions, $\bar{g}_{inhS}$ will only significantly increase across (and therefore modulate) the midpoint distribution. In contrast, under noisy background conditions, $\bar{g}_{inhS}$ will significantly increase across (and therefore modulate) the neuron dynamic range, whereas it will not do so for the narrow midpoint distribution.

homogeneous excitation under noisy background conditions (right column). Figure 4*A* shows g_{excS} curves as a function of input strength; for heterogeneous excitation, 10 different values of slope were chosen randomly from a normal distribution and were then used for all subsequent testing. For each condition, we tested feedforward inhibition fixed at 1 mS/cm^2 and feedforward inhibition whose amplitude varied with input strength.

Figure 4*B* shows the *i*–*o* curve for each model neuron tested. As expected, neurons were recruited abruptly in the absence of noise but, since excitation was heterogeneous across neurons, they were recruited at different input strengths (Fig. 4*B*, left panels). This staggering was increased by input-dependent feedforward inhibition (cf. top and bottom panels). Neurons were recruited gradually under noisy conditions and, since excitation was homogeneous, all neurons were recruited across the same range of input strengths (Fig. 4*B*, right panels). This range was increased but recruitment remained unstaggered with input-dependent feedforward inhibition. The midpoint distribution and population dynamic range for each condition are shown in Figure 4*C*,*D*, respectively. Brackets shown in Figure 4 demarcate the dynamic range and help explain its regulation: For heterogeneous excitation without background noise, the dynamic range corresponds to where the steepest and shallowest g_{excS} curves enter the region of deterministic spiking (solid gray in Fig. 4*A*); for homogeneous excitation and noise, the dynamic range corresponds to where the g_{excS} curve enters and exits the region of probabilistic spiking (gray gradient in Fig. 4*A*). Notably, when g_{inhS} co-varies with g_{excS}, the boundaries defining deterministic and probabilistic spiking become slanted; this is not shown in Figure 4*A* for sake of clarity, but the slanted threshold can be seen in Figure 5*B*.

Consistent with Figure 3, these simulations show that a broad population dynamic range can be achieved through heterogeneous excitation (which is associated with a broad midpoint distribution) or through background noise (which is associated with reduced neuronal gain). In both cases, the population dynamic range can further be modulated by feedforward inhibition. The last point—that the population dynamic range is modulated by inhibition—is consistent with Pouille et al. (2009), but contrary to the assertion that this is achieved through modulation of the midpoint (which relies on heterogeneous excitation), we have shown here that the effect can also be achieved through modulation of neuronal gain (which relies on background noise). The 2 conditions—heterogeneous excitation and background noise—are not mutually exclusive, but does one effect predominate? Based on in vivo patch clamp recordings (Lee et al. 2006; Harvey et al. 2009; Epsztein et al. 2011), CA1 pyramidal neurons exhibit spontaneous membrane potential fluctuations with a standard deviation between 2 and 4 mV. We have conservatively focused on noise near the bottom of that range. Figure 5*A* shows how neuron dynamic range varies with background noise intensity (plotted in terms of the resulting membrane potential fluctuations). From this, we conclude that neuron dynamic range is necessarily broad under the noisy conditions omnipresent in the awake brain, especially when feedforward inhibition is input-dependent.

That still does not exclude heterogeneous excitation from contributing to the population dynamic range. Regarding this point, one must consider that electrical stimulation of Schaffer collaterals does not necessarily mimic the recruitment of presynaptic CA3 neurons by natural stimulation; by extension, electrical stimulation experiments do not demonstrate that excitation is heterogeneous under physiological conditions. That said, heterogeneous activation of CA3 neurons is likely if only because of the background noise that must also exist in CA3. Therefore, using input-dependent inhibition, we combined the background noise and heterogeneous excitation tested in Figure 4 to answer how their effects combine. The resulting population dynamic range was broad (Fig. 5*B*) but little more than with

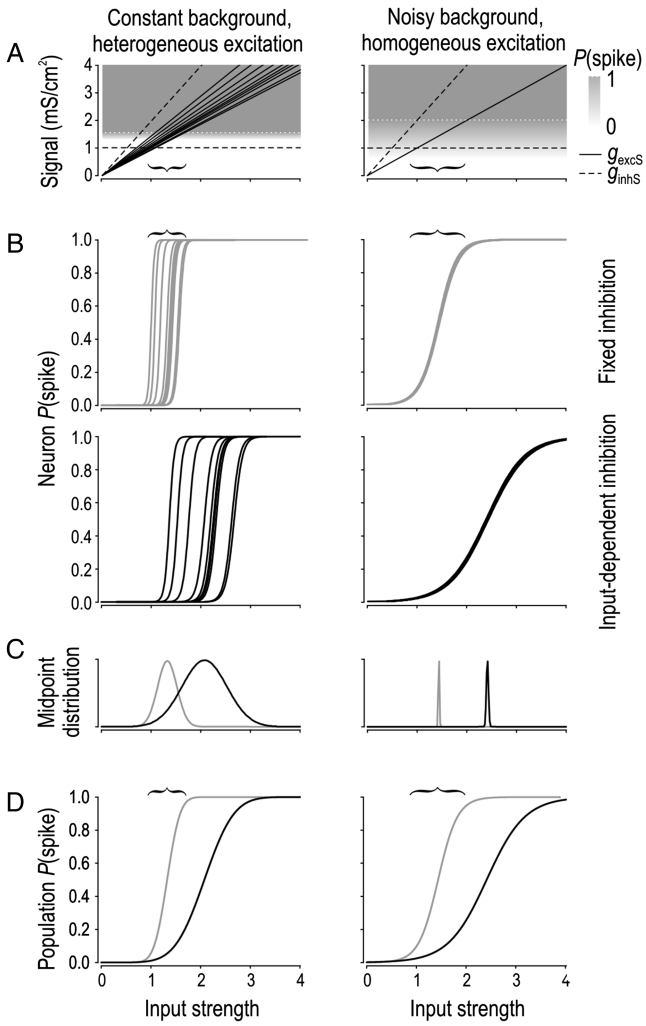

Figure 4. Computer simulations demonstrating how feedforward inhibition interacts with heterogeneous excitation and background noise to modulate dynamic range. Background input parameters (see Materials and Methods) were chosen based on experimental data in Figure 2. All tests were repeated for constant background and heterogeneous excitation (left column) and for noisy background and homogeneous excitation (right column). (*A*) Strength of excitatory signal $\bar{g}_{excS}$ (solid lines) and inhibitory signal $\bar{g}_{inhS}$ (dashed line) relative to "input strength," which is an arbitrary scale. $\bar{g}_{inhS}$ was 1 mS/cm^2 ("fixed inhibition") or increased with input strength ("input-dependent inhibition"). Probability of signal-evoked spiking is depicted with gray shading but, for clarity, is shown only for the fixed inhibition condition; input-dependent inhibition causes the bottom boundary of gray shading to become slanted (see Fig. 5*B* for example). Brackets shown in this panel help relate the slope and distribution of g_{excS} curves with the dynamic range highlighted by brackets in subsequent panels. (*B*) Neuron i–o curves were steep in the absence of noise, but were staggered when excitation was heterogeneous (left panels). Neuron i–o curves were shallower under noisy conditions (right panels). Compared with fixed inhibition (gray curves; top panels), input-dependent inhibition (black curves; bottom panels) increased the staggered recruitment in heterogeneous excitation conditions, whereas it further reduced the slope of neuron i–o curves in the noisy background condition. (*C*) Gaussian fit of midpoint distribution based on *B*. For heterogeneous excitation, the midpoint distribution was broad and was expanded by input-dependent inhibition. For homogeneous excitation, the midpoint distribution was narrow and was shifted by input-dependent inhibition. (*D*) Population i–o curves derived from data in *B* and *C* based on the methodology described in Figure 3.

homogeneous excitation. The neuron and population dynamic ranges under different conditions are summarized in Figure 5C. Under noisy conditions, the neuron dynamic range accounts for almost all of the population dynamic range even when excitation is heterogeneous; in other words, although heterogeneous excitation affects dynamic range under quiescent conditions (by broadening the midpoint distribution), that effect is almost entirely occluded by noise. The same was observed for low-conductance noisy conditions (data not shown). We ascribe this occlusion to the fact that g_{excS} curves with different slopes enter the zone of deterministic spiking (under quiescent conditions) with broad spacing, whereas the same curves enter the zone of probabilistic spiking (under noisy conditions) more tightly spaced. The latter spacing is especially narrow compared with how long it takes a typical g_{excS} curve to traverse the zone of probabilistic spiking (under noisy conditions), whereas the former spacing is especially wide compared with how abruptly g_{excS} curves enter the zone of deterministic spiking (under quiescent conditions). In other words, the zone of probabilistic spiking created by noise dampens the impact of heterogeneous excitation. This explanation applies equally to the effects of heterogeneous cellular excitability and, indeed, the occlusion noted here is reminiscent of that observed in Figure 3. These results argue that heterogeneous synaptic excitation has appreciable effects only in the absence of noise; since noise is omnipresent in the intact brain, it logically follows that heterogeneous excitation has little effect on dynamic range in the intact brain.

Signal-Evoked Spikes to Remain Precisely Timed Despite Noise

Although noise expands the dynamic range of individual neurons and thereby allows the network to have a broad dynamic range that is beneficial for coding on the basis of the rate (or, equivalently, the probability) of spiking, such noise may be expected to compromise coding that relies on precise spike timing. Given that precisely timed spikes do occur and are thought to play an important role in hippocampal coding (Harris et al. 2002; Mehta et al. 2002; Huxter et al. 2003; Dragoi and Buzsaki 2006; Shapiro and Ferbinteanu 2006; Harvey et al. 2009; Schmidt et al. 2009; Takahashi and Sakurai 2009; Diba et al. 2014), we returned to dynamic clamp experiments to investigate whether precise spike timing could occur under the noisy conditions expected in vivo.

To investigate this, we compared the timing of signal-evoked spikes under different conditions. Figure 6A shows sample responses from a typical neuron given just-maximal stimulation, defined as the weakest EPSG yielding *P*(spike) > 0.9. Bottom panels show the cumulative probability of spiking as a function of latency from stimulus onset where "jitter" is quantified as the time window for *P*(spike) to rise from 0.1 to 0.9. Jitter was predictably highest under noisy conditions but signal-evoked spikes still occurred when the EPSG was at or near its peak. Evoked spikes occurred after the onset of the IPSG but during its rising phase, consistent with Pouille et al. (2009). The spike latency distribution under noisy conditions remained narrower than might be expected from the significantly broadened distribution of voltages at signal onset ($P < 0.001$; Kolmogorov–Smirnov test; Fig. 6B). But, compared with responses to just-maximal stimulation within the same cell under noisy conditions, responses to supramaximal stimulation exhibited less jitter while submaximal stimulation exhibited more jitter (Fig. 6C). Additional experiments were conducted with >500 trials/cell so that even weak signals yielded >100 spikes, thus enabling the cumulative probability distribution of spike latencies to be accurately measured even at low *P*(spike) value; $\bar{g}_{excS}$ was adjusted to give a different *P*(spike) in each neuron. These data for submaximal stimulation confirmed that jitter is inversely correlated with *P*(spike), but

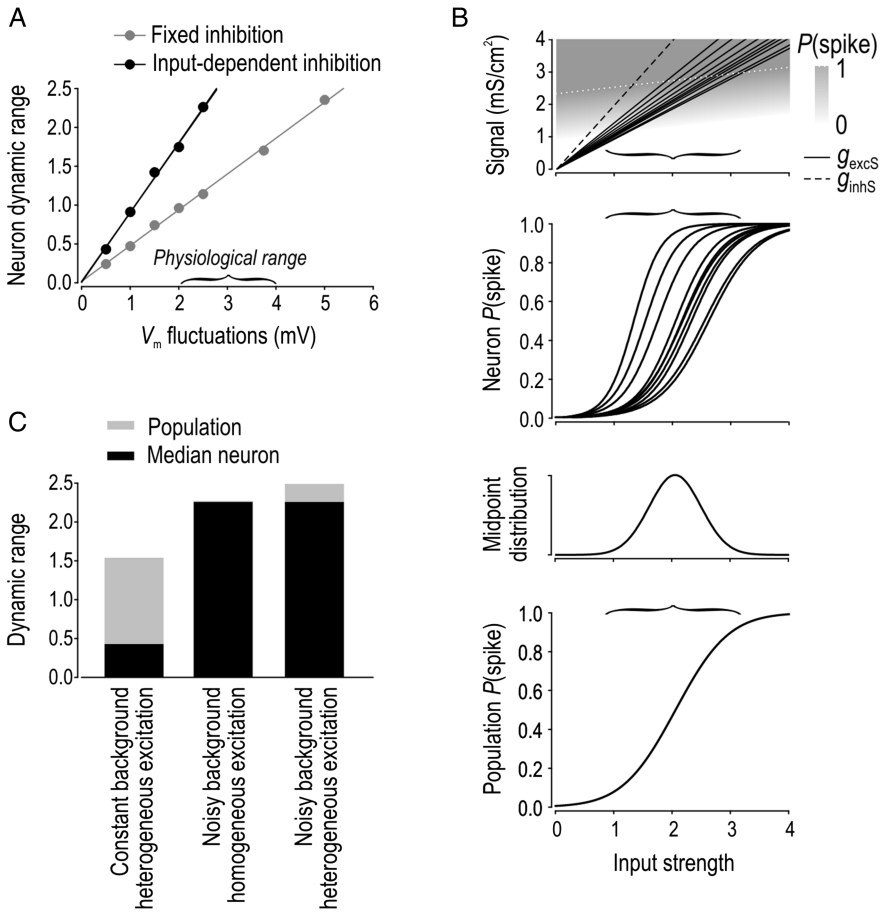

Figure 5. Computer simulations to test relative impact of heterogeneous excitation and background noise on population dynamic range. (*A*) Neuron dynamic range (defined by the input range over which *P*(spike) rises from 0.05 to 0.95) is plotted against noise amplitude quantified by the standard deviation of resultant membrane potential fluctuations. Dynamic range increases linearly with voltage fluctuation amplitude ($r^2 = 0.99$). The slope of that relationship is modulated by feedforward inhibition. (*B*) Simulations like in Figure 4 with noisy background and heterogeneous excitation. Data are shown only for input-dependent inhibition, which is why the gray border is slanted. Notably, the dynamic range is not much larger than that observed for the comparable conditions but with homogeneous excitation. (*C*) Summary of neuron and population dynamic range for different combinations of excitation heterogeneity and background conditions, with input-dependent inhibition in all cases. Whereas heterogeneous excitation produced a broad population dynamic range when neuron dynamic range was narrow, it did little to expand the population dynamic range when neuron dynamic range was broad because of noise. These data argue that the effect of background noise on dynamic range occludes the effect of heterogeneous excitation.

reaches a ceiling near 6 ms (Fig. 6*D*). Based on within-cell jitter of about 1.5 ms without noise, we conclude that noise can increase jitter by up to 4.5 ms when the signal is weak. This is consistent with previous work in neocortical neurons (Rodriguez-Molina et al. 2007).

To understand the population response, one must, of course, also consider the variability in spike latency across neurons due to cellular heterogeneity. We therefore compared the spike latency distribution across different neurons tested with just-maximal stimulation (Fig. 6*E*). Between-neuron jitter (quantified as the range of median latencies; see arrows in Fig. 6*E*) was around 2 ms in the absence of noise, but was reduced to 1.6 ms under noisy conditions. This noise-mediated reduction in between-neuron jitter results from spike latencies being skewed toward a minimal latency of about 2.5 ms; spikes occurring at shorter latencies represent purely noise-induced (i.e., signal-independent spikes). The same analysis applied to cells reported in Figure 6*D* revealed between-neuron jitter of only 1.4 ms despite those neurons exhibiting a range of *P*(spike) values. This occurs because as *P*(spike) gets lower, within-cell jitter increases mostly on account of a minority of spikes occurring at longer latencies, which means that the median latency (and its variance across neurons) is relatively unaffected. Next, we plotted the spike latency distribution for each set of neurons to visualize the cumulative effects of within- and between-neuron jitter under each test condition (Fig. 6*F*). According to these population responses, jitter under control and constant background conditions were 2.1 and 2.3 ms, respectively, and increased to 2.9 ms for noisy background with just-maximal stimulation, and to 4.2 ms for noisy background with submaximal stimulation. In other words, for a set of neurons receiving a common signal but independent noise, noise at most doubles the jitter, but the resulting spike timing is still within a range likely to reliably evoke spiking in neurons further downstream (Galan et al. 2008). Furthermore, Figure 6*F* shows that few spikes occurred later than 8 ms under any condition, consistent with feedforward inhibition acting to ensure the fidelity of signal-evoked spiking (Pouille and Scanziani 2001; Dubruc et al. 2013). But unlike its regulation of spike timing, feedforward inhibition does not prevent background noise from increasing membrane potential variance across trials (and

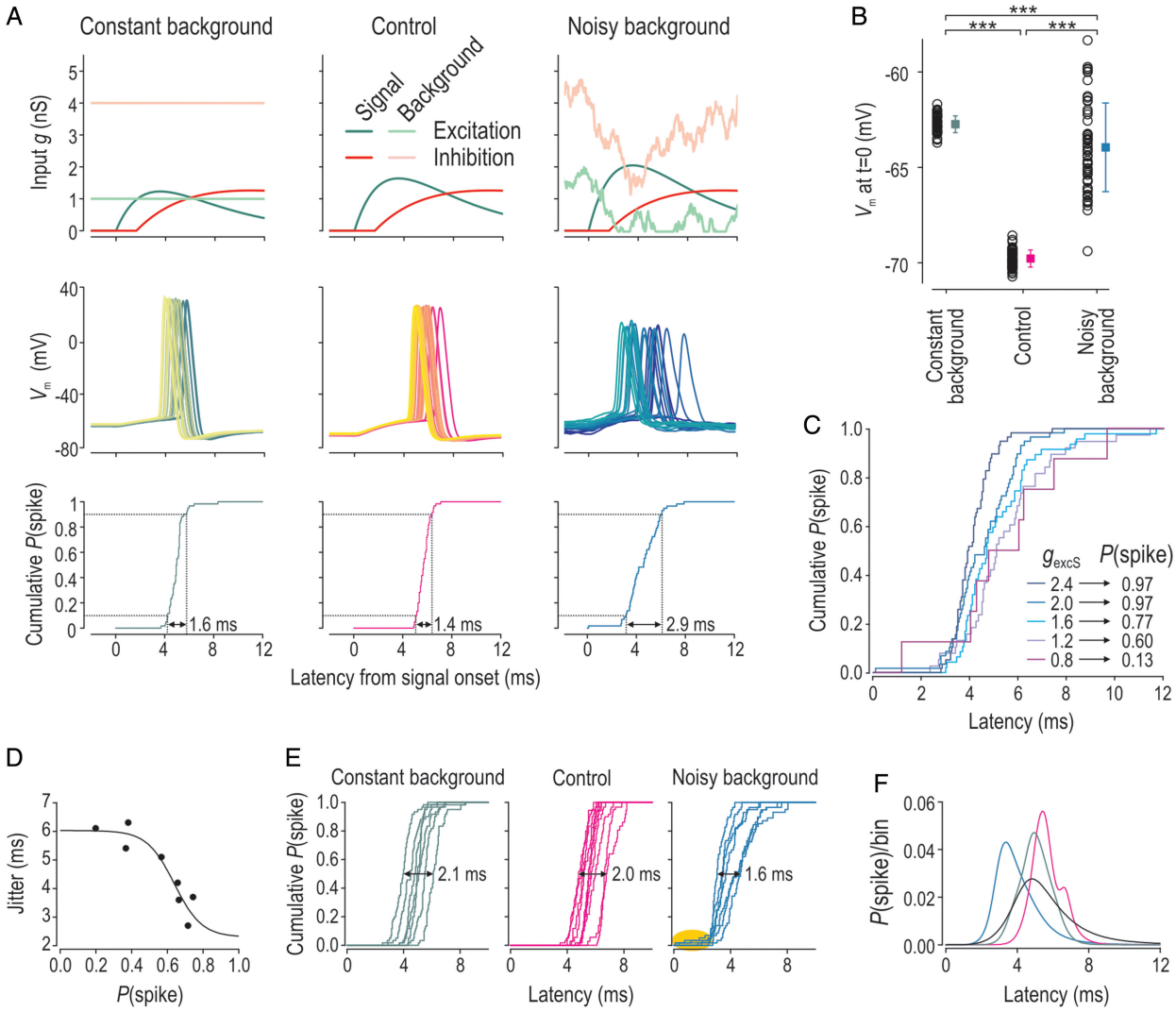

Figure 6. Effects of background conditions on spike timing and membrane potential. (*A*) Sample responses from the cell illustrated in Figure 2A to just-maximal stimulation defined as the weakest $\bar{g}_{excS}$ yielding *P*(spike) > 0.9: $\bar{g}_{excS}$ = 1.2, 1.6, and 2.0 nS for constant background, control, and noisy background, respectively. Top row shows EPSG and IPSG (i.e., signal) plus background. Only one instantiation of noisy background is shown since noise differs on each trial. Middle row shows spiking response from every third trial superimposed on each other, where coloring progresses from lightest to darkest based on membrane potential (V_m) at the time of signal onset (i.e., *t* = 0 ms). Bottom row shows cumulative probability distribution of spike latencies. Dotted lines mark the 10th and 90th percentile range that we use to quantify "jitter." (*B*) Membrane potential at signal onset for each trial (open circles). Mean ± SD for each condition is shown in color. Constant and noisy background both caused a significant shift in mean membrane potential (***$P < 0.001$, Kolmogorov–Smirnov test) compared with control. Comparing between constant and noisy background revealed a significant difference in membrane potential variance (***$P < 0.001$, Kolmogorov–Smirnov test). (*C*) Cumulative probability distribution of spike latencies for the range of signal intensities ($\bar{g}_{excS}$) tested under noisy conditions. Stronger $\bar{g}_{excS}$ is associated with shorter median spike latency and less jitter. (*D*) Jitter plotted against *P*(spike) based on neurons tested with several hundred signal events (Fig. 7). Curve shows sigmoidal fit constrained to pass through 2.3 ms, which is the average within-neuron jitter for all neurons tested with just-maximal stimulation under noisy conditions. (*E*) Cumulative probability distribution of spike latencies for each neuron tested in response to just-maximal stimulation. Distribution of the median latency across neurons is highlighted by arrows, and defines between-neuron jitter. Yellow shading in right panel highlights purely noise-induced spiking that occurs at a low rate of 2–5 Hz. (*F*) Distribution of spike latencies based on all neurons tested under each condition. Colored curves correspond to conditions illustrated in *E*; black curve corresponds to cells analyzed in *D* (noisy background with submaximal stimulation). Jitter calculated from the 10th and 90th percentile range of the corresponding cumulative probability distributions (not shown) was: control, 2.1 ms; constant background, 2.3 ms; noisy background with just-maximal stimulation, 2.9 ms; noisy background with submaximal stimulation, 4.2 ms.

between neurons) and it is, ultimately, this variance that allows weak EPSGs to evoke a spike on some trials while preventing strong EPSGs from evoking spikes on all trials, thus resulting in a shallow i–o curve.

Modulation of Signal-Evoked Spiking by Noise

In a final set of experiments, we investigated how noise modulates signal-evoked spiking by identifying what aspects of the noise are correlated with the presence or absence of spikes. To do this, we conducted additional experiments in which each neuron was tested between 510 and 765 times with a signal whose $\bar{g}_{excS}$ was adjusted to give *P*(spike) values between 0.2 and 0.8. Using these data, signal-triggered ensembles of g_{excN} and g_{inhN} were collected for each neuron; each ensemble was then subdivided into "hits" and "misses" according to whether a spike was or was not evoked on that trial. From this, we calculated 4 signal-triggered averages (STAs) for each neuron. Figure 7A shows

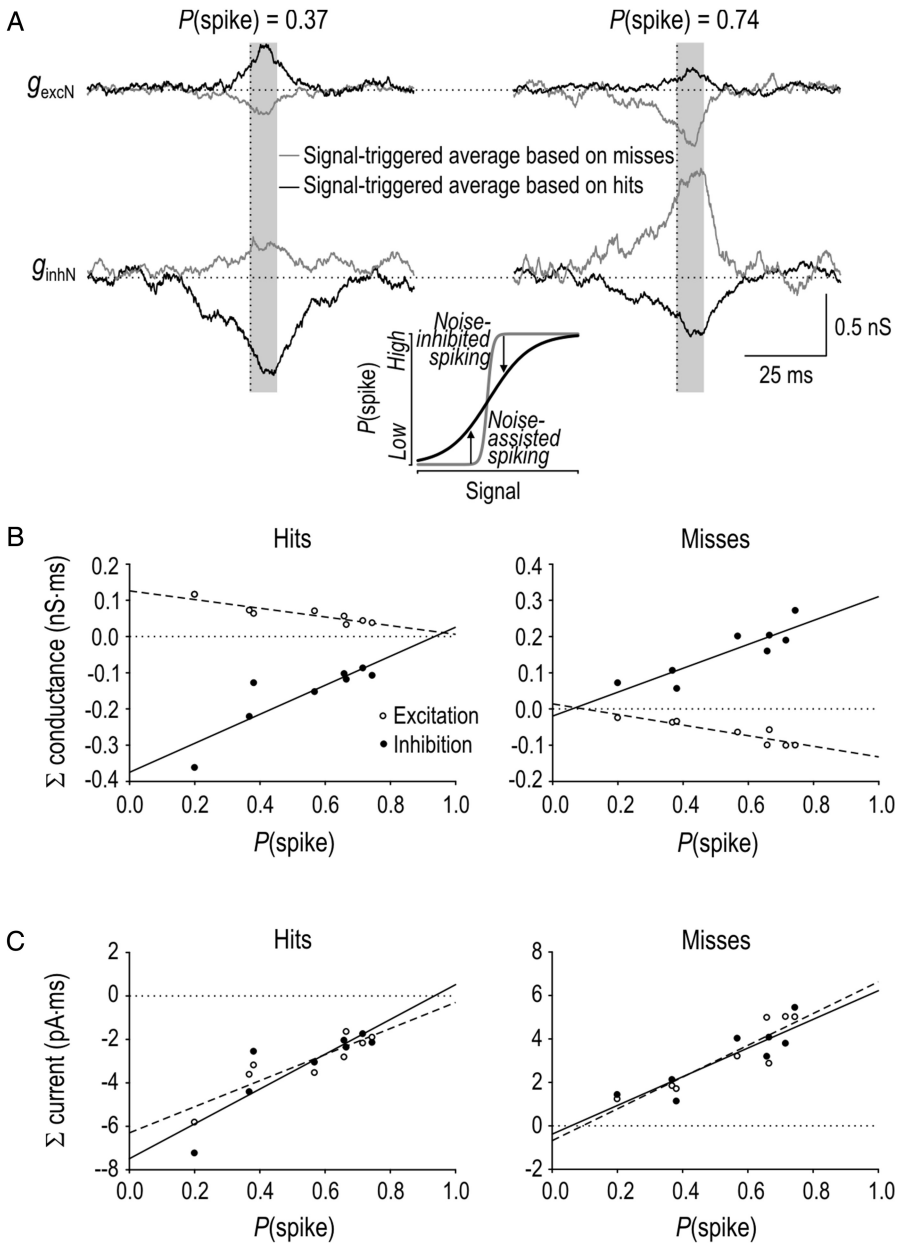

Figure 7. Effects of noise on signal-induced spiking. (*A*) Representative STAs of g_{excN} and g_{inhN} from 2 neurons with different *P*(spike). Each signal-triggered ensemble was subdivided into "hits" (black) and "misses" (gray) according to whether or not the signal evoked a spike on a given trial. Note that hits are associated with increased g_{excN} and decreased g_{inhN}, whereas misses are associated with the opposite pattern. Moreover, "hit"-STAs are larger than "miss"-STAs when *P*(spike) is low, whereas the opposite is true when *P*(spike) is high, consistent with noise assisting or inhibiting signal-evoked spiking (see inset). The constant component of the background noise (g_{exc0} and g_{inh0}) were subtracted such that STAs show deviations above or below this average (horizontal dotted lines). The vertical dotted line shows the time of signal onset and gray shading demarcates the 8-ms-long window during which most spikes occur. (*B*) Plotting STA size, quantified as the area under the curve, against *P*(spike) confirms that noise encourages spiking when *P*(spike) is low and discourages spiking when *P*(spike) is high. (*C*) STAs of g_{excN} and g_{inhN} were converted to currents (I_{excN} and I_{inhN}) by multiplying by a driving force of −50 mV and +20 mV, respectively, based on critical effects occurring within a perithreshold voltage range between −55 and −45 mV (mean = −50 mV). Plotting the area under these converted STAs against *P*(spike) revealed that cells are equally sensitive to changes in background input mediated by synaptic excitation or inhibition.

representative STAs from 2 neurons. Misses were associated with reduced g_{excN} and increased g_{inhN} (i.e., net inhibition), whereas hits were associated with the opposite pattern (i.e., net excitation). All STAs had approximately the same shape but hit-STAs were larger than miss-STAs for neurons with low *P*(spike), but the opposite was true for neurons with high *P*(spike). This relationship was quantified by plotting the area under each STA as a function of *P*(spike) (Fig. 7*B*). The relationships make sense insofar as noise encourages signal-evoked spiking when the signal is not strong enough to produce spikes on its own, whereas noise discourages spiking when the signal is strong enough to produce spikes on its own. This is the basis for smoothing an otherwise steep *i*–*o* relationship (Gammaitoni 1995); notably, the noise responsible for this effect must be independent across the set of neurons that receive a common signal. By multiplying the STAs of the conductance by driving force, STAs were

converted to current. The results demonstrate that neurons are equally sensitive to fluctuations in excitatory or inhibitory current (Fig. 7C). This contrasts the results of Rudolph et al. (2007), who observed that reduced inhibition had a stronger effect than increased excitation but, in their case, disinhibition itself drove spiking rather than modulating the effects of a separate signal. We have simulated g_{excN} and g_{inhN} as processes that are uncorrelated with each other and with the signal, but noise arising within a structured network could exhibit correlations. It is conceivable that one or the other component of the noise could become more important, or that their relative timing could play a role, under certain conditions.

The above results demonstrate that background noise, whether through increases or decreases in excitatory or inhibitory input, can encourage or discourage signal-evoked spiking. Notably, noise STAs are protracted compared with the narrow window associated with signal-evoked spiking (Fig. 6F). This suggests that fluctuations in background input that straddle the time during which the signal arrives will influence the likelihood of the signal evoking a spike, but it is the time course of the signal rather than that of the noise that dictates the timing of the spikes, consistent with our interpretation of data in Figure 6.

Discussion

This study explains how the dynamic range of the CA1 pyramidal neuron population is regulated under the noisy conditions that exist in the intact, awake brain. Notably, our results overturn claims (Pouille et al. 2009) that CA1 pyramidal neurons have steep *i*–*o* curves, and that the CA1 population achieves its broad dynamic range by staggering the abrupt recruitment of individual neurons. The aforementioned mechanism applies only under the unnaturally quiescent conditions that prevail in slice preparations, where background synaptic activity is minimal. When we reintroduced natural levels of noisy background input, the same neurons that had exhibited steep *i*–*o* curves under control conditions now exhibited shallow *i*–*o* curves. Therefore, under the noisy conditions existing in the awake brain, individual neurons have broad and overlapping dynamic ranges. Moreover, noise was found to occlude the effects of heterogeneous excitation, meaning staggered recruitment of individual neurons does not contribute significantly to the population dynamic range. Similarly, heterogeneities in cellular excitability had only a small effect compared with that of background synaptic noise. Our results also demonstrated that feedforward inhibition broadens the dynamic range of individual neurons, which, in turn, serves to broaden the population dynamic range. And finally, we showed that noise that is sufficient to produce a broad dynamic range does not preclude precisely timed spiking. Overall, these results suggest that naturally occurring levels of background noise can benefit rate coding without disrupting temporal coding, consistent with previous demonstrations of the beneficial effects of noise, or what has been referred to as "stochastic facilitation" [for review, see McDonnell and Ward (2011)]. In both cases, feedforward inhibition plays an important role—by operating as a gain control mechanism in the context of rate coding and by limiting spike latencies in the context of temporal coding.

Consistent with previous studies on the effects of shunting inhibition (see Introduction), adding a constant conductance shifted the *i*–*o* curve without affecting its slope, which is attributable to the shift in mean prestimulus membrane potential (Fig. 6B). However, when the conductance was made realistically noisy, its main effect was to reduce the slope of the neuron *i*–*o* curve, which is attributable to the increased variance of prestimulus membrane potential (Fig. 6B). Notably, taking advantage of the benefits afforded by our dynamic clamp-based stimulation, we varied only the EPSG amplitude (controlled by $\bar{g}_{excS}$) for the purpose of plotting *i*–*o* curves since allowing the IPSG amplitude (controlled by $\bar{g}_{inhS}$) to co-vary with the EPSG would have further expanded the dynamic range (Fig. 5A). Thus, for experiments, we excluded the effect of co-varying inhibition and isolated the effects of noise on the neuron *i*–*o* curve.

One must appreciate that the shape of the *i*–*o* curve affects how that curve is modulated. When the starting *i*–*o* curve is shallow (e.g., because of noisy background input), balanced increases in the EPSG and IPSG will delay the full recruitment of the neuron, reducing the slope of the *i*–*o* curve rather than controlling at what stimulus intensity the neuron is abruptly recruited. In contrast, when the *i*–*o* curve is very steep, balanced increases in the EPSG and IPSG will delay the recruitment of a neuron until a disproportionate increase in the EPSG occurs, as per the explanation of Pouille et al. (2009). Importantly, our data do not argue that excitation is homogeneous across neurons; on the contrary, we expect that excitation is heterogeneous, especially under noisy conditions, but that does not mean that heterogeneous excitation is the principal determinant of the population dynamic range or that inhibition relies on heterogeneous excitation for its effects. Similarly, neurons are heterogeneous in their excitability, and this can have important implications for neural coding (Padmanabhan and Urban 2010). However, our data show that heterogeneities in synaptic excitation and in cellular excitability have little effect on the population dynamic range when individual neurons themselves have a broad dynamic range (i.e., reduced gain). Since neuronal gain is reliably reduced by even modest levels of noise, and noise is omnipresent in the awake brain, we conclude that population dynamic range is principally regulated by noise effects. This is likely the case for any brain region in which operating conditions are noisy, which most certainly includes neocortex (Destexhe et al. 2003). Indeed, previous in vitro and in vivo experiments (Chance et al. 2002; Shu et al. 2003; Cardin et al. 2008) have firmly established that neocortical pyramidal neurons tested under realistically noisy conditions have smooth *i*–*o* curves whose gain is modulable. Recent in vivo experiments in visual cortex have shown that parvalbumin-expressing interneurons (unlike somatostatin-expressing interneurons) modulate the response gain of pyramidal neurons (Atallah et al. 2012; Wilson et al. 2012); earlier studies have already shown that such an effect relies on the noisy conditions present in vivo [see discussion in Prescott and De Koninck (2003)].

For an input that is so brief that only a single spike per neuron can occur during it (which is the scenario tested here and by Pouille et al. (2009)), the firing rate of the population is dictated by the number of neurons that respond with a single spike. In this scenario, each neuron responds in an all-or-none fashion (0 or 1 spikes) on any given trial, but the difference between quiescent and noisy conditions is whether the neuron has an all-or-none probability of spiking (quiescent conditions) or a graded probability of spiking (noisy conditions). This scenario is comparable to that considered by Maass and Natschläger (2000), except that probabilistic spiking is attributable to background synaptic activity in our case rather than to unreliable synaptic transmission; both forms of "noise" enable what Maass and Natschläger refer to as space-rate coding. A network comprising neurons with graded response profiles is liable to be more fault-tolerant than one comprised of neurons with all-or-none response profiles. For instance, the former network is not dependent on subtle heterogeneities in synaptic excitation to ensure staggered

neuron recruitment and a broad population dynamic range; in turn, such a network would be more robust to damage or altered operating conditions. However, one might suspect that a noisy network is incapable of supporting neural codes that depend on precise spike timing. In that respect, our demonstration (Fig. 6*F*) that spike timing remains quite precise despite high levels of background noise is notable. Specifically, we showed that for a set of neurons receiving a common signal but independent noise, noise doubled the jitter (to 4.2 ms) for submaximal signal strengths, and had an even smaller effect when signals were stronger. Even if jitter is doubled, spike timing precision remained within the range believed to drive reliable spiking in downstream neurons (Galan et al. 2008). This level of precision is also consistent with synchronization reflecting second-order stimulus statistics, as opposed to rate co-modulation reflecting first-order statistics (Hong et al. 2012).

In summary, we have shown that individual pyramidal neurons have a broad dynamic range under realistically noisy conditions. Individual neurons can, therefore, be recruited across a broad range of stimulus intensities, especially if excitation and feedforward inhibition co-vary with stimulation intensity. Under these conditions, the population dynamic range is broad because of the graded recruitment of many neurons across a broad stimulus range, not because of the staggered recruitment of neurons at specific stimulus intensities.

Funding

This work was supported by NIH grant R01 NS076706, by a Discovery Grant from the National Sciences and Engineering Research Council of Canada, by a New Investigator Award from the Canadian Institutes of Health Research, and by an Early Researcher Award from the Ontario Ministry of Research and Innovation.

Notes

We thank Tim Bergel at Cambridge Electronic Design for making modifications to the dynamic clamp software. *Conflict of Interest*: None declared.

References

Atallah BV, Bruns W, Carandini M, Scanziani M. 2012. Parvalbumin-expressing interneurons linearly transform cortical responses to visual stimuli. Neuron. 73:159–170.

Bernander O, Douglas RJ, Martin KA, Koch C. 1991. Synaptic background activity influences spatiotemporal integration in single pyramidal cells. Proc Natl Acad Sci USA. 88:11569–11573.

Blomfield S. 1974. Arithmetical operations performed by nerve cells. Brain Res. 69:115–124.

Broicher T, Malerba P, Dorval AD, Borisyuk A, Fernandez FR, White JA. 2012. Spike phase locking in CA1 pyramidal neurons depends on background conductance and firing rate. J Neurosci. 32:14374–14388.

Cardin JA, Palmer LA, Contreras D. 2008. Cellular mechanisms underlying stimulus-dependent gain modulation in primary visual cortex neurons in vivo. Neuron. 59:150–160.

Chance FS, Abbott LF, Reyes AD. 2002. Gain modulation from background synaptic input. Neuron. 35:773–782.

Destexhe A, Paré D. 1999. Impact of network activity on the integrative properties of neocortical pyramidal neurons in vivo. J Neurophysiol. 81:1531–1547.

Destexhe A, Rudolph M, Fellous JM, Sejnowski TJ. 2001. Fluctuating synaptic conductances recreate in vivo-like activity in neocortical neurons. Neuroscience. 107:13–24.

Destexhe A, Rudolph M, Paré D. 2003. The high-conductance state of neocortical neurons in vivo. Nat Rev Neurosci. 4:739–751.

Diba K, Amarasingham A, Mizuseki K, Buzsaki G. 2014. Millisecond timescale synchrony among hippocampal neurons. J Neurosci. 34:14984–14994.

Dragoi G, Buzsaki G. 2006. Temporal encoding of place sequences by hippocampal cell assemblies. Neuron. 50:145–157.

Dubruc F, Dupret D, Caillard O. 2013. Self-tuning of inhibition by endocannabinoids shapes spike-time precision in CA1 pyramidal neurons. J Neurophysiol. 110:1930–1944.

Eccles JC. 1964. The physiology of synapses. Berlin: Springer.

Epsztein J, Brecht M, Lee AK. 2011. Intracellular determinants of hippocampal CA1 place and silent cell activity in a novel environment. Neuron. 70:109–120.

Ermentrout B. 2002. Simulating, analyzing, and animating dynamical systems: a guide to XPPAUT for researchers and students. Philadelphia: SIAM.

Fernandez FR, White JA. 2010. Gain control in CA1 pyramidal cells using changes in somatic conductance. J Neurosci. 30: 230–241.

Galan RF, Ermentrout GB, Urban NN. 2008. Optimal time scale for spike-time reliability: theory, simulations, and experiments. J Neurophysiol. 99:277–283.

Gammaitoni L. 1995. Stochastic resonance and the dithering effect in threshold physical systems. Phys Rev E. 52: 4691–4698.

Harris KD, Henze DA, Hirase H, Leinekugel X, Dragoi G, Czurko A, Buzsaki G. 2002. Spike train dynamics predicts theta-related phase precession in hippocampal pyramidal cells. Nature. 417:738–741.

Harvey CD, Collman F, Dombeck DA, Tank DW. 2009. Intracellular dynamics of hippocampal place cells during virtual navigation. Nature. 461:941–946.

Ho N, Destexhe A. 2000. Synaptic background activity enhances the responsiveness of neocortical pyramidal neurons. J Neurophysiol. 84:1488–1496.

Holmes WR, Woody CD. 1989. Effects of uniform and non-uniform synaptic "activation-distributions" on the cable properties of modeled cortical pyramidal neurons. Brain Res. 505:12–22.

Holt GR, Koch C. 1997. Shunting inhibition does not have a divisive effect on firing rates. Neural Comput. 9:1001–1013.

Hong S, Ratté S, Prescott SA, De Schutter E. 2012. Single neuron firing properties impact correlation-based population coding. J Neurosci. 32:1413–1428.

Huxter J, Burgess N, O'Keefe J. 2003. Independent rate and temporal coding in hippocampal pyramidal cells. Nature. 425:828–832.

Lee AK, Manns ID, Sakmann B, Brecht M. 2006. Whole-cell recordings in freely moving rats. Neuron. 51:399–407.

Longtin A, Doiron B, Bulsara AR. 2002. Noise-induced divisive gain control in neuron models. Biosystems. 67:147–156.

Maass W, Natschläger T. 2000. A model for fast analog computation based on unreliable synapses. Neural Comput. 12:1679–1704.

McDonnell MD, Ward LM. 2011. The benefits of noise in neural systems: bridging theory and experiment. Nat Rev Neurosci. 12:415–426.

Mehta MR, Lee AK, Wilson MA. 2002. Role of experience and oscillations in transforming a rate code into a temporal code. Nature. 417:741–746.

Mitchell SJ, Silver RA. 2003. Shunting inhibition modulates neuronal gain during synaptic excitation. Neuron. 38:433–445.

Morris C, Lecar H. 1981. Voltage oscillations in the barnacle giant muscle fiber. Biophys J. 35:193–213.

Padmanabhan K, Urban NN. 2010. Intrinsic biophysical diversity decorrelates neuronal firing while increasing information content. Nat Neurosci. 13:1276–1282.

Pouille F, Marin-Burgin A, Adesnik H, Atallah BV, Scanziani M. 2009. Input normalization by global feedforward inhibition expands cortical dynamic range. Nat Neurosci. 12: 1577–1585.

Pouille F, Scanziani M. 2001. Enforcement of temporal fidelity in pyramidal cells by somatic feed-forward inhibition. Science. 293:1159–1163.

Prescott SA, De Koninck Y. 2003. Gain control of firing rate by shunting inhibition: roles of synaptic noise and dendritic saturation. Proc Natl Acad Sci USA. 100:2076–2081.

Prescott SA, De Koninck Y. 2009. Impact of background synaptic activity on neuronal response properties revealed by stepwise replication of in vivo -like conditions in vitro. In: Destexhe A, Bal T, editors. The dynamic clamp: from principles to applications. New York: Springer. p. 89–114.

Prescott SA, De Koninck Y, Sejnowski TJ. 2008. Biophysical basis for three distinct dynamical mechanisms of action potential initiation. PLoS Comput Biol. 4:e1000198.

Prescott SA, Ratté S, De Koninck Y, Sejnowski TJ. 2006. Nonlinear interaction between shunting and adaptation controls a switch between integration and coincidence detection in pyramidal neurons. J Neurosci. 26:9084–9097.

Prescott SA, Ratté S, De Koninck Y, Sejnowski TJ. 2008. Pyramidal neurons switch from integrators in vitro to resonators under in vivo-like conditions. J Neurophysiol. 113: 2242–2249.

Ratté S, Hong S, De Schutter E, Prescott SA. 2013. Impact of neuronal properties on network coding: roles of spike initiation dynamics and robust synchrony transfer. Neuron. 78:758–772.

Rodriguez-Molina VM, Aertsen A, Heck DH. 2007. Spike timing and reliability in cortical pyramidal neurons: effects of EPSC kinetics, input synchronization and background noise on spike timing. PLoS ONE. 2:e319.

Rudolph M, Pospischil M, Timofeev I, Destexhe A. 2007. Inhibition determines membrane potential dynamics and controls action potential generation in awake and sleeping cat cortex. J Neurosci. 27:5280–5290.

Schmidt R, Diba K, Leibold C, Schmitz D, Buzsaki G, Kempter R. 2009. Single-trial phase precession in the hippocampus. J Neurosci. 29:13232–13241.

Shapiro ML, Ferbinteanu J. 2006. Relative spike timing in pairs of hippocampal neurons distinguishes the beginning and end of journeys. Proc Natl Acad Sci USA. 103:4287–4292.

Shu Y, Hasenstaub A, Badoual M, Bal T, McCormick DA. 2003. Barrages of synaptic activity control the gain and sensitivity of cortical neurons. J Neurosci. 23:10388–10401.

Silver RA. 2010. Neuronal arithmetic. Nat Rev Neurosci. 11: 474–489.

Takahashi S, Sakurai Y. 2009. Sub-millisecond firing synchrony of closely neighboring pyramidal neurons in hippocampal CA1 of rats during delayed non-matching to sample task. Front Neural Circuits. 3:9.

Uhlenbeck GE, Ornstein LS. 1930. On the theory of Brownian motion. Phys Rev. 36:823–841.

Wilson NR, Runyan CA, Wang FL, Sur M. 2012. Division and subtraction by distinct cortical inhibitory networks in vivo. Nature. 488:343–348.

Wolfart J, Debay D, Le Masson G, Destexhe A, Bal T. 2005. Synaptic background activity controls spike transfer from thalamus to cortex. Nat Neurosci. 8:1760–1767.